Arabian Journal of Chemistry (2021) **14**, 102952

King Saud University

Arabian Journal of Chemistry

www.ksu.edu.sa
www.sciencedirect.com

ORIGINAL ARTICLE

Corrosion behaviors of Q235 carbon steel under imidazoline derivatives as corrosion inhibitors: Experimental and computational investigations

Liping Xiong [a], Pengjie Wang [a], Zhongyi He [a,*], Qi Chen [a], Jibin Pu [b], Renhui Zhang [a,*]

[a] *School of Materials Science and Engineering, East China JiaoTong University, Nanchang 330013, People's Republic of China*
[b] *Key Laboratory of Marine Materials and Related Technologies, Zhejiang Key Laboratory of Marine Materials and Protective Technologies, Ningbo Institute of Materials Technology and Engineering, Chinese Academy of Sciences, Ningbo 315201, People's Republic of China*

Received 17 October 2020; accepted 13 December 2020
Available online 21 December 2020

KEYWORDS

Imidazoline derivatives;
Weight loss;
Electrochemical experiments;
Theoretical calculation

Abstract In this work, two new imidazoline derivatives were successfully synthesized, and the molecular structure of which has been proved by IR, Raman and elemental analysis. The corrosion inhibition performance of the imidazoline derivatives for carbon steel in 3.5 wt% sodium chloride simulation-concrete-pore solution was investigated. The weight loss and electrochemical test results exhibited that compared to the blank systems, the corrosion inhibition efficiency was effectively enhanced with increasing the concentrations of two imidazoline derivatives, the maximum corrosion inhibition efficiency of weight-loss test is 96.02%. The inhibition efficiency of Electrochemical impedance spectroscopy and Potentiodynamic polarization were 95.95% and 90.69%. EDS analysis confirmed that two new imidazoline derivatives could effectively adsorb on the Q235 steel surface, which was further supported by density functional theory (DFT) and molecular dynamics simulations. This work confirmed that two new imidazoline derivatives exhibited a potential application in engineering and equipment.

1. Introduction

Owing to its superior mechanical performance and low cost, the application of reinforced Q235 steel bar was a common practice in many concrete structure industries, which exhibited superior weight capacity (Zhang et al., 2019). In terms of its application environments, especially for buildings around/in ocean, due to the existence of micro-pores in concrete buildings, the chloride ions easily permeated and reacted with

* Corresponding authors.
E-mail addresses: zhyhe@ecjtu.edu.cn (Z. He), 3067@ecjtu.edu.cn (R. Zhang).
Peer review under responsibility of King Saud University.

ELSEVIER Production and hosting by Elsevier

https://doi.org/10.1016/j.arabjc.2020.102952
1878-5352

Q235 steel bar, which further corroded Q235 steel bar, the corrosion products will cause concrete cracking and spalling, which will lead to the decline of mechanical properties of concrete, and eventually lead to the collapse of buildings, which not only endangers the safety of the structure but also brings huge economic losses. Thus, reducing or even eliminating the corrosion of reinforced concrete is of great significance (Liu et al., 2020).

Many new materials and technologies have been developed with an objective to increase the service life of reinforced concrete structures. These methods including chloride extraction, cathodic protection, application of protective coatings and sealers, concrete re-alkalization and use of corrosion inhibitors, can prevent and mitigate the corrosion of steel in concrete. Among the available methods, the using of corrosion inhibitors is one of the most convenient, attractive and cost-effective method to prevent corrosion of steel in concrete (Ferkous et al., 2020).

Based on the mechanism of action, corrosion inhibitors can be divided into two types: anode type and cathode type, which can control the anodic reaction and cathodic reaction, as long as one of the electrodes is suppressed, the corrosion rate can be effectively reduced. Anodic corrosion inhibitors (typically, chromate, nitrite and molybdate) can prevent or slow down the anodic process employing forming "protective films" on the surface of reinforced steels (Rbaa et al., 2020). For example, nitrite has been widely used as the main component of corrosion inhibitors in the early stage because of its excellent corrosion inhibiting effect. However, the downside of the nitrite inhibitor is that local corrosion and accelerated corrosion will occur when the concentration of chloride ions reaches a certain level, which makes nitrite inhibitor known as dangerous corrosion inhibitor. Besides, nitrite inhibitor is infamous for carcinogenic alkali aggregate reaction, which significantly affects the slump (Pan et al., 2020).

Cathodic corrosion inhibitors, such as zincate, phosphate and organic compounds, prevent or slow down the cathodic process through forming a passive film via adsorption, but most of which are not effective when used alone. Thus, a lot of research on a mixture of different types of corrosion inhibitors have been reported, which usually focus on a reasonable combination of cathode type, anode type, increasing resistance type, reducing oxidation type and other substances. Such mixing corrosion inhibitors have good rust resistance and low toxicity, but its synthesis method and process are complicated. It should be noted that the addition of a large number of different types of corrosion inhibitors mixture into the concrete cannot guarantee uniform distribution of each type on the surface of steel.

It has been reported that imidazoline can play an excellent corrosion inhibition performance in concrete (Xu et al., 2020; Kousar et al., 2019; Finšgar, 2020). Imidazoline quaternary ammonium salt is easier to adsorb on the surface of Q235 steel to form a protective film and play a excellent corrosion inhibition effect (Cao et al., 2019; Pakiet et al., 2019). It was reported that the combination of iodine ion and corrosion inhibitor could improve the corrosion inhibition efficiency (Aquino-Torres et al., 2020; Tan et al., 2020). Therefore, the fabrication of imidazoline derivatives was a feasible way to improve and enhance the anticorrosion performance of Q235 steel.

Generally speaking, these inhibitors have multiple adsorption sites, which can play an excellent corrosion inhibition performance in the concrete inhibitor molecules. According to the literatures, According to the literatures (Yu et al., 2019), Zongxue Yu research the inhibition efficiency of benzoyl lauric acid imidazoline quaternary ammonium salt was 91.19%, and its active sites were mainly distributed on imidazole ring and phenyl. Its active sites were not as many as SMIF inhibitor, and its inhibition performance was much higher than that of benzoyl lauric acid imidazoline quaternary ammonium salt. Penggang Wang research (Wang et al., 2020) the inhibition efficiency of the inhibitor is 88.73%, and the adsorption sites of the inhibitor are not as many as those of SMIF inhibitor, and the corresponding inhibition effect is not as high as that of SMIF inhibitor. SMIF inhibitors also contain iodine ions, which can also play a certain inhibition effect. This inhibitor molecule can play a good corrosion inhibition performance.

In this work, two new imidazoline derivatives were synthesized, their microstructures and anti-corrosion performances were examined by IR, Raman, NMR and electrochemical methods. The morphologies of Q235 steel after weight loss tests were characterized by SEM and ESD technique. In addition, density functional theory (DFT) and molecular dynamics (MD) simulation were employed to provide a molecular level insights into the inhibition mechanism.

2. Experimental and computational methods

2.1. Experimental methods

2.1.1. Preparation of SMIF and SMID

The compounds SMIF and SMID were synthesized in the laboratory. The oleic imidazoline was synthesized by oleic acid and diethylenetriamine, and then n-phenylthiourea and n-methylthiourea were added after adding 1-iodobutane, respectively, to form SMIF and SMID. The specific steps are as follows: oleic acid and diethylenetriamine were added into a four-port flask at a molar ratio of 1:1.1, heated at 140 °C for 2 h, then dehydrated at 190–210 °C to cyclize. Subsequently, xylene was used to carry the water out of the reaction system and refluxed for 1.5 h to fully separate the water and diethylenetriamine. After adding 1-iodobutane, n-phenylthiourea and n-methylthiourea was added respectively, and reacted for 1.5 h, The target product could be synthesized when the temperature was kept around 140 °C and cooled to room temperature. Finally, the products were vacuum distilled to separate other impurities in the system (Rbaa et al., 2020; Bashir et al., 2020; Cao et al., 2017). The chemical synthesis roadmap of it is shown in Scheme 1.

2.1.2. Materials

The corrosion inhibition experiments were carried out on the Q235 with the following composition (wt.%): C: ≤0.22%, Mn: ≤1.4%, Si: ≤0.35%, S: ≤0.050%, P: ≤0.045%, and Fe (for balance). Q235 steel was cut into the suitable size (12 mm × 12 mm × 2 mm, 10 mm × 10 mm × 30 mm) which were utilized for weight loss testing, surface analysis and electrochemical analysis. Before setting up the experiment, these coupons were ground using different grades of emery paper (80–2000 grade) and degreased with anhydrous ethanol and air-dried. These coupons were then preserved in a vacuum desiccator for further corrosion measurements and electrochemical measurements (Zhang et al., 2019).

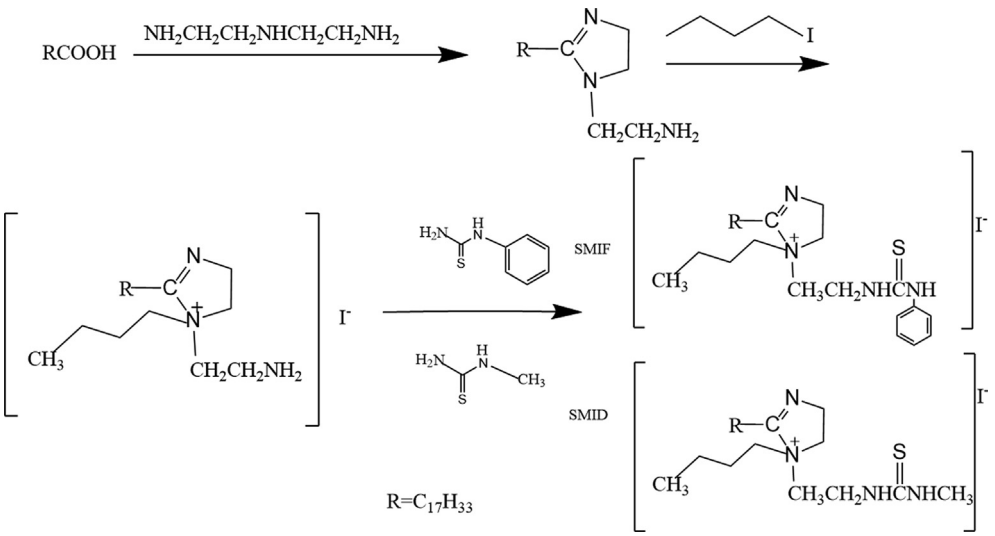

Scheme 1 Reaction roadmap of imidazoline derivatives synthesis.

Inhibition experiments were carried out in a synthetic concrete pore solution: 0.6 mol/L potassium hydroxide + 0.2 mol/L sodium hydroxide + saturated calcium hydroxide solution with 3.5 wt% NaCl, (SCP solution) (Zhang et al., 2019; Chen et al., 2019). Four different concentrations SMIF and SMID were considered: 0.0; 1.0, 2.0, 3.0, and 4.0 g/L.

All the chemical reagents mentioned in this paper are from Aladdin reagent network. Oleic acid: ≥99.0% (GC); Diethylenetriamine: greater than 99% (GC); 1-iodobutane: greater than 98.0% (GC); n-methylthiourea: 98%; n-phenylthiourea: 98%. Inorganic reagent: AR

2.1.3. Weight loss analysis

For weight loss measurements, the above mentioned the carbon steel samples with dimensions 12 mm × 12 mm × 2 mm were used. These samples were initially weighted down before setting up the experiment and then careful immersed in a 200 ml beaker of test solution retained at a temperature range of 298 K in a temperature-controlled oven. After 5 days of immersion time, these samples were taken out and wiped off with acetone then air-dried and final weight of the samples noted down to analyze the weight loss. The weight loss measurement was achieved by calculating the difference in the weight loss of the steel samples before and after immersion in a blank solution. Various parameters as corrosion rate and corrosion inhibition efficiency were calculated via this method.

The inhibition efficiency $\eta(\%)$ and corrosion rate C_R were calculated using Eqs. (1)–(2):

$$C_R(\mathrm{mgcm^{-2}h^{-1}}) = \frac{\Delta w}{A \cdot t} \quad (1)$$

$$\eta(\%) = \frac{C_{R(0)} - C_{R(i)}}{C_{R(0)}} \times 100 \quad (2)$$

where Δw, A, t represent weight loss of inhibited and uninhibited specimens (mg), surface area of specimens (cm^2) and immersion time (h), respectively. $C_{R(0)}$ and $C_{R(i)}$ represent the corrosion rates in uninhibited and inhibited cases.

2.1.4. Electrochemical tests

All the electrochemical experiments were performed on an electrochemical workstation (PARSTAT 2273) in a three-electrode-type vessel. This three-electrode consisted of a saturated calomel electrode (SCE) (the reference electrode (RE)), a 1 cm^2 Pt plate (the auxiliary electrode (CE)) and the Q235 specimens with the size of 10 mm × 10 mm × 30 mm (the working electrode (WE)). The WE with 1 cm^2 exposing surface area was treated before electrochemical experiments: abrading with emery paper from 80 to 2000 grade in turn then rinsing gently with adequate distilled water, washing with absolute ethyl alcohol. The WE was immersed in SCP solution for 900 s to attain a stable value of open circuit potential (OCP), when testing OCP, the immersing time of carbon steel in solution is 3600 s, then using Potentiodynamic polarization (Tafel) technology and electrochemical impedance spectroscopy (EIS) measurement and polarization tests, the immersing time was 120 s and 900 s. The EIS measurements were then performed based on OCP with an amplitude signal of 10 mV in the frequency range from 100 kHz down to 50 mHz. All the abtained EIS data were fitted using ZSimwin 3.10 software (EChem Software). Polarization studies were performed at ± 250 mV vs SCE at OCP and the sweep rate is 0.25 mV/s. Generally, the sweep speed of 0.25 mV/s, which can better show the polarization corrosion in the corrosion system. Corrosion current density (i_{corr}) values were calculated from the obtained polarization curves using Tafel extrapolation (Berisha, 2020). All the electrochemical tests were carried out at 25 °C.

2.1.5. Characterization methods

Characterization of corrosion inhibitors: the IR spectrum and ATR-FTIR spectrum (Spectrum One PE: USA) measurements were carried out within the working range of 500–4000 cm^{-1}. The Raman spectrum (DXR) measurements were carried out within the working range of 600–2600 cm^{-1}. The inhibitor molecules were characterized by 1H NMR spectra and 13C NMR spectra (AVANCE 400).

The carbon steel specimens immersed in SCP solution with presence and absence of inhibitor was used to investigate sur-

face analysis by scanning electron microscopy (SEM: X Flash Detector 5010 BRUKER Nano) (Saraswat et al., 2020).

2.2. Computational methods

Quantum chemical calculations were conducted using the software of Materials Studio (Accelrys Ltd.). The geometrical optimizations calculations were chosen and completed on the cation of SMIF and SMID molecule with DMol3 module based on the density functional theory (DFT) (Ye et al., 2020; Asadi et al., 2020). The molecular dynamics (MD) simulation of SMIF and SMID molecules on the Fe surface was also investigated. The iron crystal was imported and cleaved along the Fe plane first and then a slab of 10 Å was employed. The simulations had been done with condensed-phase optimized molecular potentials for atomistic simulation studies (COMPASS) force field that were suitable for chemical and condensed-phase systems (Ye et al., 2020; Asadi et al., 2020). The MD simulation was conducted in a simulation box (Å $10 \times 10 \times 40$), which uses the Forcite module using a NVT canonical ensemble with a total simulation time of 500 ps and a time step of 5 fs, at 298 K (Ye et al., 2020; Asadi et al., 2020).

3. Results and discussions

3.1. Corrosion inhibitor characterization

3.1.1. IR analysis

The IR result of SMIF and SMID are given in Fig. 1. From the Fig. 1, 3275.0 cm^{-1} (N—H str.), 1650.0 cm^{-1} (C═N str.), 1650–1640 cm^{-1} (C═C str.), 1170.0 cm^{-1} (C═S str.), 2925.0 cm^{-1} and 2842.0 cm^{-1} (CH2 str.), 1460.0 cm^{-1} (C—C str.), 1250–950 cm^{-1} (phenyl str.), 2900 cm^{-1} (CH3 str.) are belongs to the corresponding functional groups in additives (Ye et al., 2020; Asadi et al., 2020).

3.1.2. Raman analysis

The Raman result of SMIF and SMID are given in Fig. 2. From the Fig. 2, 1600, 1400 cm^{-1} (phenyl str.), 1300 cm^{-1} (CH_2 str.), 1650–1950 cm^{-1} (N—H str.), 1170.0 cm^{-1}(C═S str.), 1080 cm^{-1}(C═N str.) are belongs to the corresponding functional groups in additives (Guerrab et al., 2020).

3.1.3. Physical performance

The boiling point of SMIF is 158.0 °C and SMID is 178.5 °C. The inhibitor molecules are not soluble in water.

3.1.4. NMR analysis

The structure of SMIF and SMID were further characterized by 13C nuclear magnetic resonance (NMR) spectroscopy.

The 1H NMR spectra and 13C NMR spectra of inhibitor molecules shown in Fig. 3 From the 1H NMR spectra in Fig. 3, where δ (3.25) is the hydrogen characteristic peak of —C═N in imidazoline inhibitor, δ (7.70) is the hydrogen characteristic peak of 1-benzene. δ (7.43) is the hydrogen characteristic peak of 1 —N C═S, and δ (2.16) is the hydrogen characteristic peak of —C═C. From the 13C NMR spectra in Fig. 3, where δ (129.0) is the carbon characteristic peak of -N- C═S, δ (128.4) is the carbon characteristic peak of 1-benzene, δ (42.1) is the carbon characteristic peak of 1 beta —C(═S)—N, and δ (32.9) is the hydrogen characteristic peak of —N═C. According to the NMR of SMIF inhibitor molecule, it can be estimated that the inhibitor molecules was be synthesized successfully.

Fig. 4 displayed 1H NMR spectra and 13C NMR spectra of SMID, where δ (7.5) is the hydrogen characteristic peak of aldimine, δ (3.55) is the hydrogen characteristic peak of —NC(═S), δ (3.25) is the hydrogen characteristic peak of —C═N. δ (2.16) is the hydrogen characteristic peak of 1 —C═C,and δ (1.25) is the hydrogen characteristic peak of methylene.

From the Fig. 4 13C NMR spectra, where δ (130.6) is the carbon characteristic peak of 1-ethylene, δ (28.0) is the carbon characteristic peak of —C═N and δ (15.2) is the carbon characteristic peak of 1 beta —C(═S)—N.

According to the NMR of SMIF and SMID inhibitor molecule. It can be explained that the inhibitor molecules can be synthesized.

3.1.5. Elemental analysis

The element analysis of the corrosion inhibitor was carried out by PE 2400 II type element analyzer. The element contents of

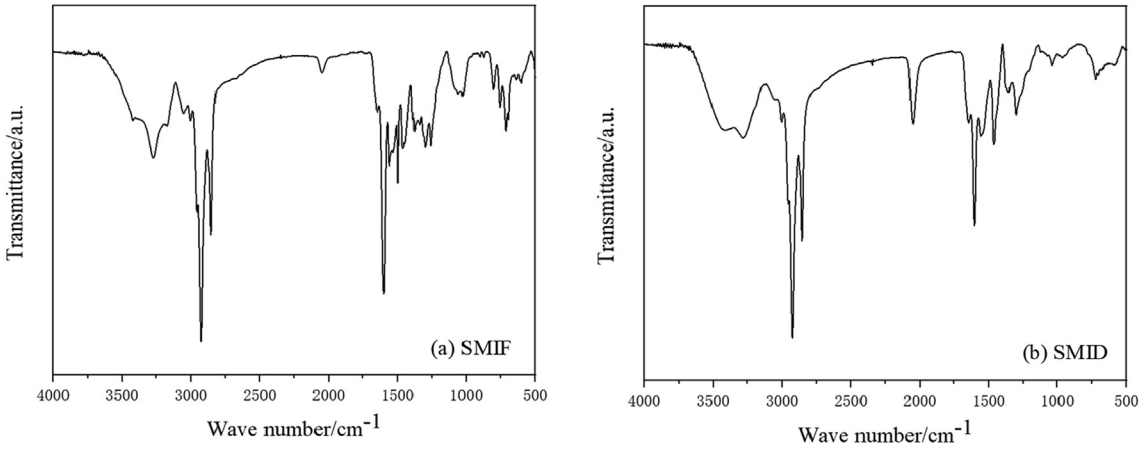

Fig. 1 IR spectrum of SMIF (a) and SMID (b).

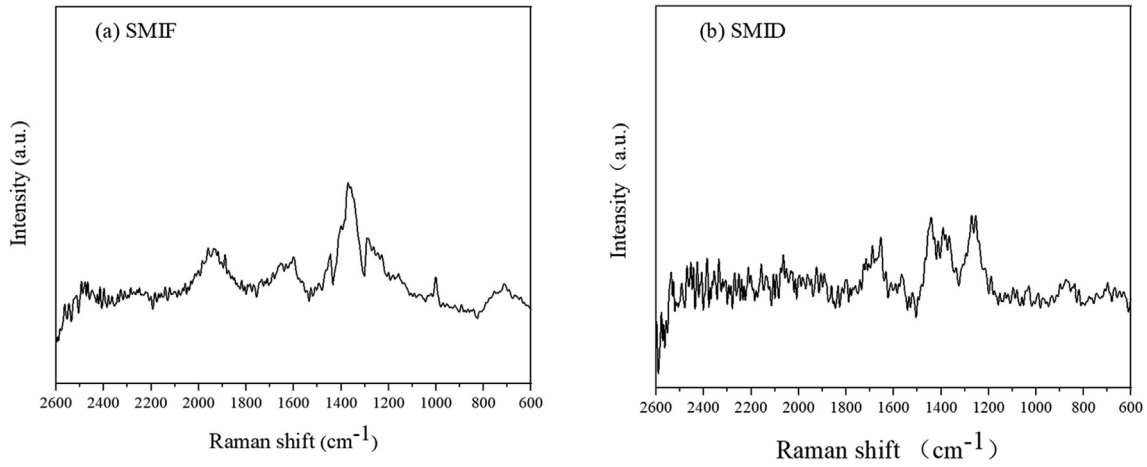

Fig. 2 Raman spectrum of SMIF (a) and SMID (b).

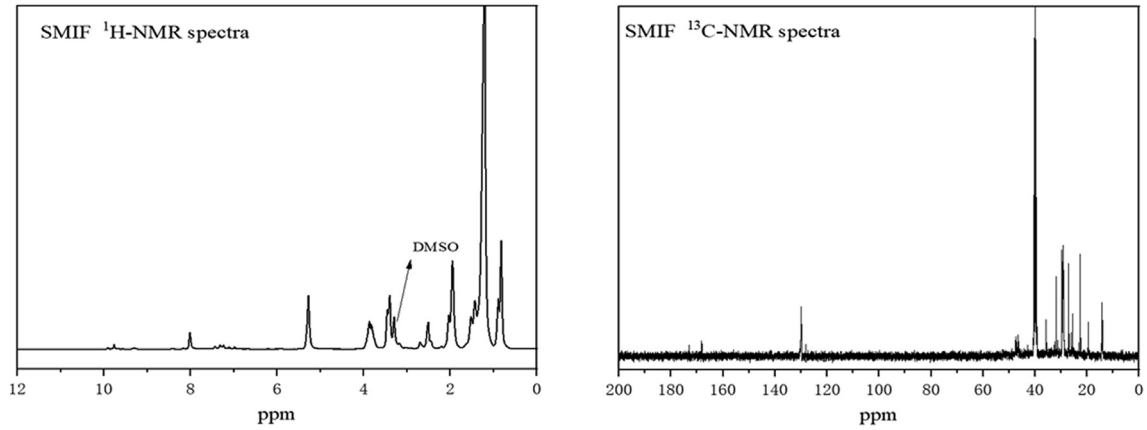

Fig. 3 NMR spectra of inhibitor molecules: ^{1}H NMR spectra of SMIF in DMSO (left), ^{13}C NMR spectra of SMIF in DMSO (right).

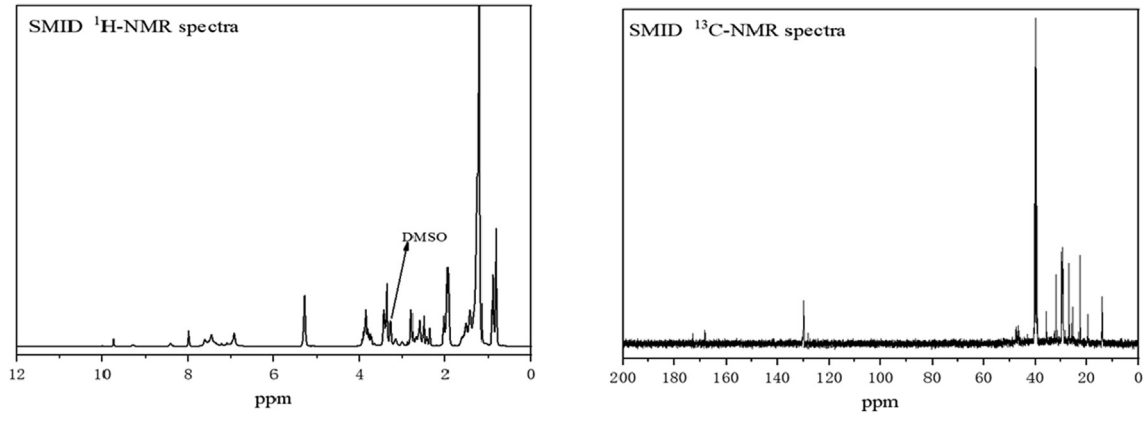

Fig. 4 1 NMR spectra of inhibitor molecules: ^{1}H NMR spectra of SMID in DMSO (left), ^{13}C NMR spectra of SMID in DMSO (right).

the corrosion inhibitor are shown in Table 1. According to Table 1, the theoretical content of the inhibitor is basically consistent with the measured content. Combined with the IR and Roman analysis results, it can be concluded that the inhibitor molecules are basically synthesized.

3.2. Weight loss analysis

In order to determine the effect of corrosion inhibitor on corrosion rate and corrosion inhibition efficiency of Q235 in SCP solution, the weight loss of Q235 sample immersed in different

Table 1 The element contents of the corrosion inhibitor.

	N (%)	C (%)	S (%)	H (%)
SMIF measured value	8.38	59.60	4.56	8.72
SMIF theoretical value	9.38	59.28	4.79	9.53
SMID measured value	9.17	57.38	5.32	7.35
SMID theoretical value	9.20	57.22	5.27	7.45

content solution was studied. Each concentration was conducted three times and the average value was recorded in the various parameters shown in Table 2 (Bashir et al., 2020).

As shown in Table 2, the corrosion rate values reduced from 0.143 to 0.006 mg cm^{-2} h^{-1} when added 4.0 g/L SMIF in SCP solution. The inhibition efficiency raised to 96.02% when 4.0 g/L SMIF was immersed in SCP solution and the corrosion rate decreases with the increase of inhibitor concentration. The reduction is directly attributed to the adsorption of corrosion inhibitor molecules on carbon steel active sites. Also, by increasing additive concentration the surface coverage can be enhanced and higher inhibition performance can be attained. The inhibition efficiency of SMIF is higher than that of SMID. It may be that the adsorption strength of phenyl in SMIF is higher than that of methyl in SMID, which is more conducive to the adsorption of inhibitor molecules on the surface of carbon steel.

3.3. OCP analysis

As is known that significant attention should be paid to the stability of the open circuit potential, before each electrochemical test such as EIS, and Tafel polarization (Guo et al., 2015). The OCP values of the specimens immersed in the SCP solutions in the absence/presence of inhibitors are recorded as a function of immersion time as shown in Fig. 5

The initial decrease of OCP value in the first minutes of exposure period can ascribe to the corrosion reactions occurrence on the steel substrate. This initial drop was pronounced in the blank and inhibitor-containing solutions, and the most negative OCP values belonged to blank specimens (Padash et al., 2020). Extending the measurement time to 900 s, it was observed that samples subjected to the solutions inhibited by SMIF and SMID showed little variation at longer immersion times. This can act as a sign of the formation of a stable barrier film composed of SMIF on the steel panels, inhibiting the contact of corrosive ions and water molecules with the steel surface. Since almost constant values were achieved in different solutions after 900 s, the EIS tests and Tafel polarization were conducted after this exposure time (Yan et al., 2020).

3.4. Potentiodynamic polarization tests

Fig. 6 shows the potentiodynamic polarization curves for carbon steel with different concentrations of SMIF and SMID.

The electrochemical parameters such as corrosion potential (E_{corr}), corrosion current density (i_{corr}), anodic and cathodic Tafel slope (β_a, β_c) along with the percentage of inhibition efficiency (%*IE*) are listed in Table 3. The percentage inhibition efficiency (%*IE*) was calculated using the Eq. (3):

$$\%\mathrm{IE} = \frac{i^0_{corr} - i_{corr}}{i^0_{corr}} \tag{3}$$

where i^0_{corr} and i_{corr} are the values of corrosion current density in the absence and presence of inhibitors, respectively.

The maximum decrease in current density from 16.93 to 0.69 mA/cm2 was observed for SMIF, indicating that the inhibition efficiencies of SMIF is better than SMID as the best inhibitor. The presence of phenyl group in SMIF is resulted in its higher inhibition performance as compared to SMID (Singh et al., 2020). With the increase of inhibitor concentration, the current density decreased gradually, which proved that the inhibitor molecules adsorbed on the surface of carbon steel to form a protective film, which hindered the further corrosion of carbon steel surface by corrosive medium.

Ionic liquid molecules of inhibitors classified into anodic, cathodic or mixed type depending upon the shift in the E_{corr} values of inhibited metallic specimens for the $|E_{corr}|$ values of the uninhibited metallic specimen. In fact, the prepared organic compounds are cationic surfactants. If this displacement in $|E_{corr}|$ values are more than 85 mV then inhibitors may be categorized as cathodic or anodic type. If these displacements are less than 85 mV then inhibitors can be classified as mixed type (Douche et al., 2020). In the present case, maximum displacements in the E_{corr}values were 242 and 135 mV, indicating that SMIF and SMID acts as anodic type inhibito, which was further supported by relatively more shifts in the values of β_c as compared to the values of β_a. Inspection of Fig. 4 reveals that potentiodynamic polarization curves are parallel and similar in different concentrations of the studied

Table 2 Parameters of weightlessness experiment.

T	C	SMIF		SMID	
(K)	(g/L)	CR ($mg.cm^{-2}.h^{-1}$)	η (%)	CR ($mg.cm^{-2}.h^{-1}$)	η (%)
	blank	0.143 ± 0.005	–	0.143 ± 0.005	–
298 K	1.0	0.054 ± 0.004	62.25 ± 0.024	0.061 ± 0.005	57.34 ± 0.039
	2.0	0.033 ± 0.005	76.92 ± 0.032	0.043 ± 0.007	69.93 ± 0.050
	3.0	0.014 ± 0.005	90.21 ± 0.035	0.020 ± 0.004	86.01 ± 0.031
	4.0	0.006 ± 0.005	96.02 ± 0.034	0.010 ± 0.003	93.01 ± 0.025

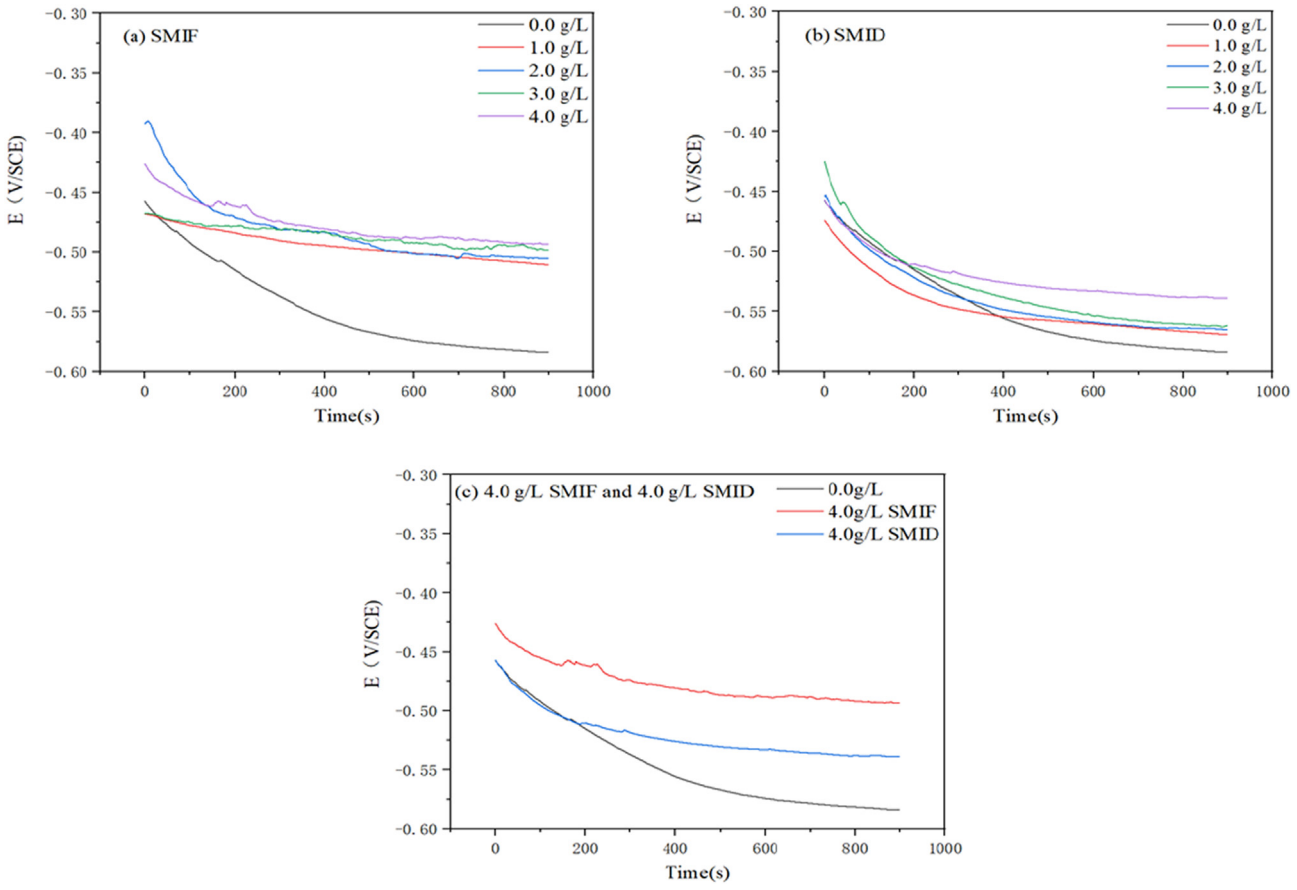

Fig. 5 Variation of the corrosion potential of carbon steel in SCP solution (a) SMIF (b) SMID (c) 4 g/LSMIF and 4 g/L SMID.

inhibitors indicating that these molecules inhibit metallic corrosion by blocking the actives sites present over the metallic surface without changing the mechanism of carbon steel corrosion (Douche et al., 2020; Sahoo et al., 2019). The mechanism of corrosion inhibition can be explained as follows: the inhibitor molecule mainly inhibits the anodic reaction, thus inhibiting the whole reaction system (Qiang et al., 2019).

3.5. Electrochemical impedance spectroscopy

Fig. 7 shows the Nyquist plots for carbon steel with different concentrations of SMIF and SMID.

Nyquist plots consist of a depressed capacitive loop along with the real axis and their size increases with increasing the concentration of inhibitor molecules (see Fig. 7), indicating that the corrosion of carbon steel in SCP solution is controlled by polarization resistance (R_p) (El Faydy et al., 2016). For a carbon steel corroding in SCP solution, R_p is associated with several types of resistances such as film resistance (R_f), solution resistance (R_s), and charge transfer resistance (R_{ct}) etc. that is $R_p = R_f + R_s + R_{ct}$.

It consists of solution resistance (R_S), film resistance (R_f), charge transfer resistance (R_{ct}) and constant phase element (CPE_f,CPE_{dl}). The impedance function of CPE can be represented by the following Eq. (4): (El-Hajjaji et al., 2018)

$$Z_{CPE} = \frac{1}{Y_0}[(j\omega)_n]^{-1} \tag{4}$$

where Y_0 and n is the magnitude and exponent (phase shift) of the CPE, respectively, $j^2 = -1$ is an imaginary number and ω is the angular frequency. Properties of CPE depend on the value of n (El-Shamy et al., 2015). n = −1, CPE stands for inductive reactance. n = 0, CPE is refer to pure resistor. n = 0.5, CPE stands for Warburg impedance. n = 1, CPE stands for pure capacitor. The C_{dl} and C_f are calculated using the following Eq. (5) (Qiang et al., 2021; Tan et al., 2021):

$$C = Y_O(\omega)^{n-1} = Y_0(2\pi f)^{n-1} \tag{5}$$

The values of EIS parameters such asR_S, R_f, CPE, Y_0 and n obtained by fitting the EIS spectra are listed in Table 4.

As shown in Table 4, the value of R_f increases and n decrease with increasing the inhibitor concentration, which is resulted of an increase in the thickness of the electrical double layer on the metal/solution interface and/or decreases in the value of dielectric constant due to the displacement of pre-adsorbed water molecules by the inhibitors. It can be seen that the values of $n_f$vary from 0.8565 to 0.6183. This parameter, which is also known as roughness and/or heterogeneity factor, can give us some useful information regarding the surface heterogeneity or geometry (roughness). It is obvious from Table 4 that in the case of without inhibitor solution. The value of n is 0.6183, indicating the increase in surface roughness as a result of severe iron dissolution. For the inhibitor-containing solutions the different concentrations of SMIF and SMID value is higher than without inhibitor, which can be demonstrated by the parameter of n. The decrease of n

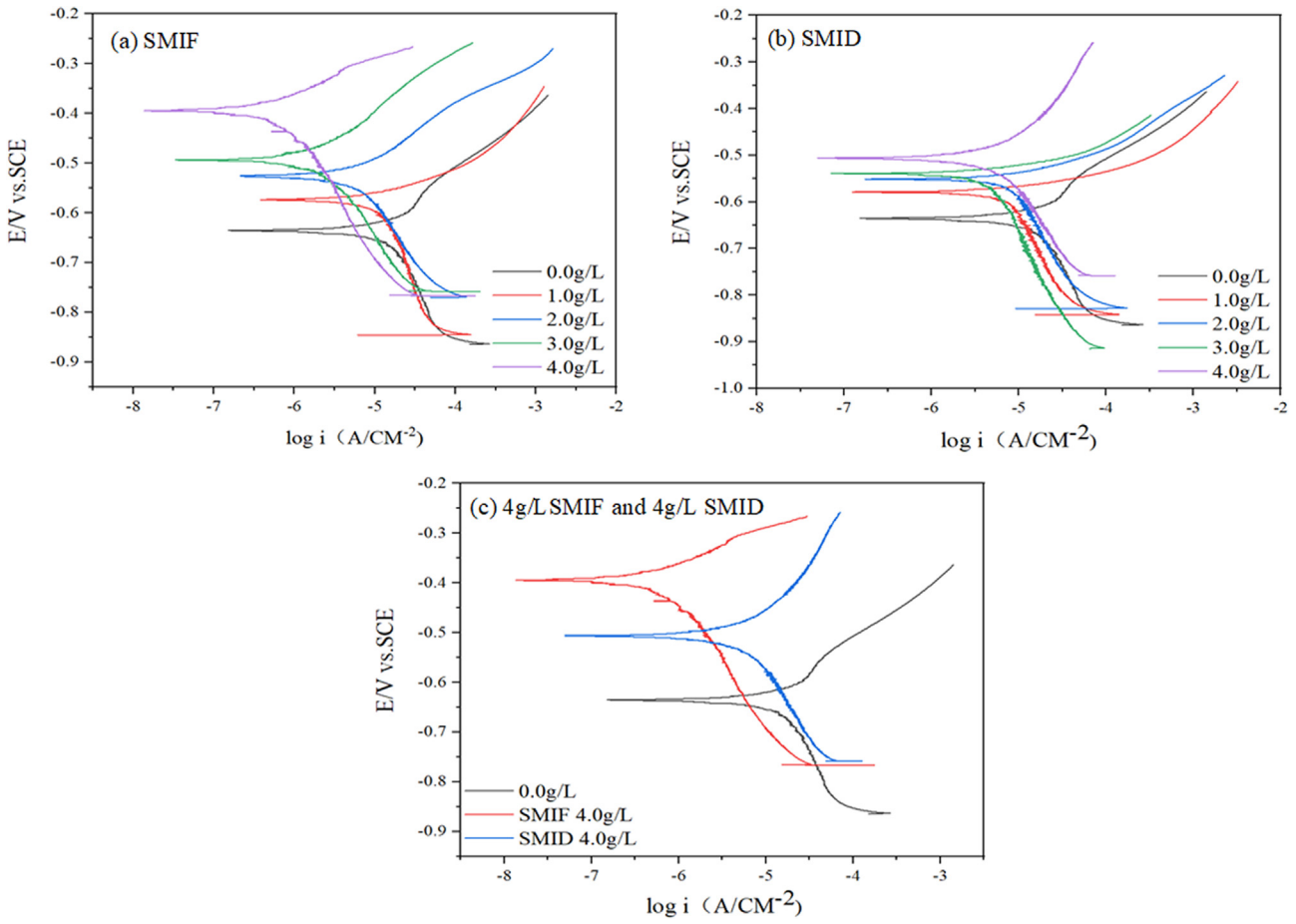

Fig. 6 Polarization curves for carbon steel corrosion in SCP solution (a) SMIF; (b) SMID; (c) 4 g/LSMIF and 4 g/L SMID.

Table 3 Potentiodynamic polarization parameters for carbon steel corrosion in the absence and presence of different concentrations of SMIF and SMID.

Inhibitors	Concentration (g/L)	E_{corr} (mV vs SCE)	i_{corr} (mA/cm^2)	β_a (mV)	β_c (mV)	η (%)
Blank	0.0	−635.394	16.93	329.959	144.48	/
SMIF	1.0	−573.571	10.02	625.685	68.818	40.81
	2.0	−526.066	5.83	471.966	169.123	65.57
	3.0	−494.150	3.02	372.804	195.373	82.19
	4.0	−393.638	0.69	245.008	103.057	95.92
SMID	1.0	−579.096	11.01	413.963	52.910	34.96
	2.0	−551.103	6.97	375.887	38.263	58.82
	3.0	−541.253	4.17	304.993	106.525	75.37
	4.0	−506.640	1.73	239.625	124.649	89.80

value can prove that the inhibitor molecules adsorb on the surface of carbon steel and inhibit the corrosion of carbon steel surface by corrosive medium, thus reducing the surface roughness of carbon steel (Cao et al., 2019; Singh et al., 2017). The values of the electric double layer capacitor (C_{dl}) and the film capacitor (C_f) show a downward trend (Tan et al., 2020). This indicates that the SMIF and SMID molecules replace the H_2O molecules on the Fe electrode surface to forming a dense anti-corrosion film (Qiang et al., 2020; Tan et al., 2019).

From Fig. 8, the inhibition performance of molecules: SMIF > SMID. The fluctuation range of R_S value is too small to be ignored, the great changes of R_f and R_{ct}can be explained that SMIF and SMID corrosion inhibitor molecules adsorb on the surface of carbon steel, forming an adsorption protective film, effectively delaying the rate of metal corrosion. It suggests that corrosion inhibition occurs by adsorption of SMIF and SMID molecules at metal interfaces. The equivalent circuit model used to interpret the impedance results is given in Fig. 9.

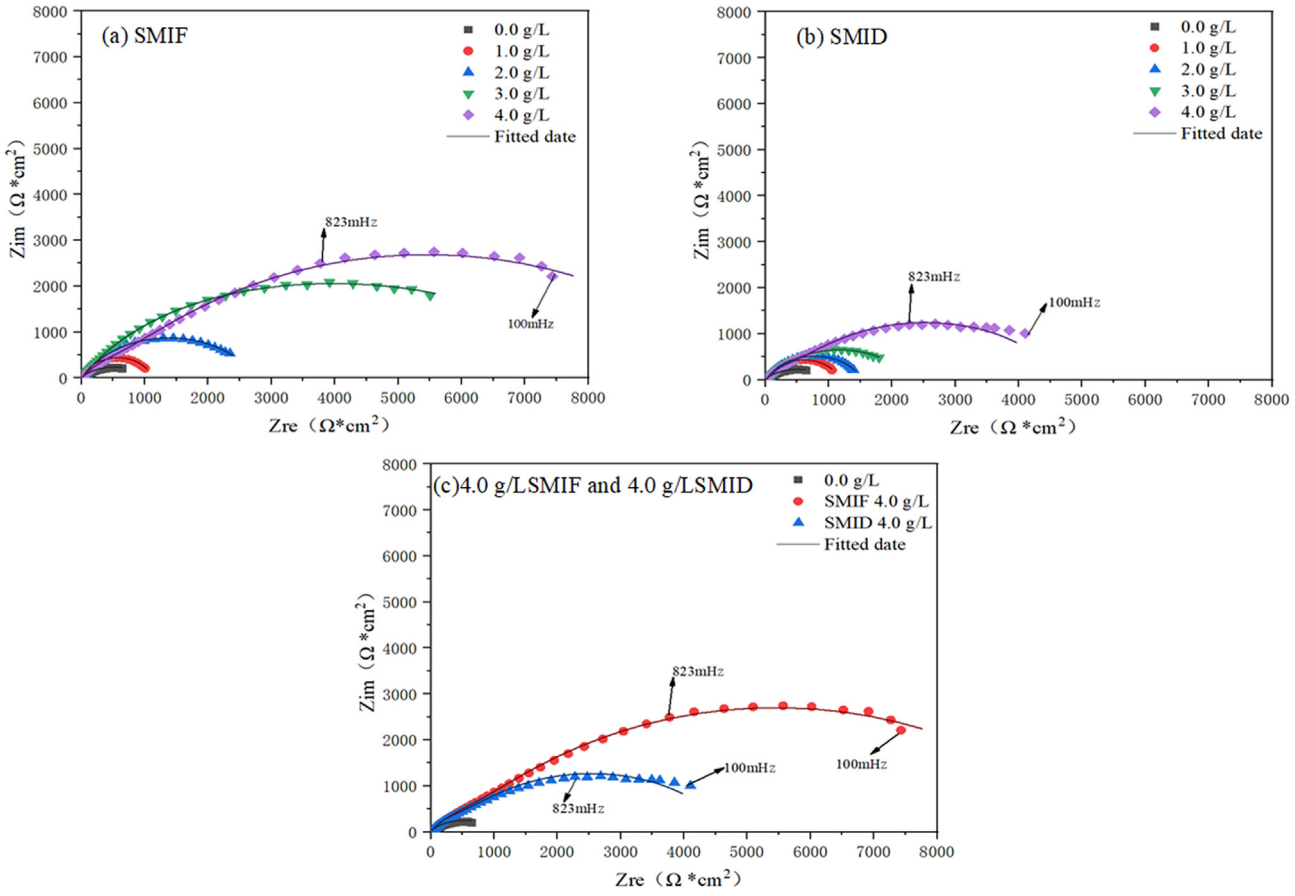

Fig. 7 Nyquist plots for carbon steel corrosion in SCP solution (a) SMIF (b) SMID (c) 4 g/LSMIF and 4 g/L SMID.

Table 4 Electrochemical impedance parameters for carbon steel corrosion in the absence and presence of different concentrations of SMIF and SMID.

Inhibitors	C (g/L)	R (Ω cm)	$Y_f * 1^{-5}$ (Ω^{-1} cm^{-2} s^n)	n_f	R_f (Ωcm^2)	Cf (μF cm^{-2})	$Y_{Rct} * 1^{-5}$ (Ω^{-1} cm^{-2} s^n)	n_2	R_{ct} (Ωcm^2)	Cdl (μF cm^{-2})	R_P Ω	η_p (%)	χ^2
Blank	0.0	10.24	182.1	0.6183	648	23.64	91.26	0.6099	322.8	14.14	981	/	0.003767
SMIF	1.0	10.71	28.15	0.8565	1073	20.47	48.60	0.8710	21.72	9.84	1105	12.91	0.006206
	2.0	10.94	12.75	0.7162	2729	13.81	4.584	0.7860	17.14	7.18	2757	64.65	0.002550
	3.0	12.70	40.66	0.6907	3468	14.88	7.929	0.6753	4538	5.50	8018	87.87	0.003344
	4.0	11.14	3.771	0.6701	5326	6.62	6.22	0.6275	9903	3.37	15,240	90.69	0.001592
SMID	1.0	11.09	89.00	0.6098	490	20.6	46.87	0.8894	713	11.1	1214	19.29	0.002830
	2.0	11.29	15.62	0.7598	1500	14.73	72.10	0.6384	21.83	7.95	1533	36.20	0.002277
	3.0	11.69	22.87	0.6588	2275	13.9	27.94	0.6490	18.8	7.18	2305	57.68	0.002393
	4.0	11.47	9.451	0.6540	4354	7.01	4.073	0.7378	381.6	3.87	4747	78.49	0.003128

Zsimwin software is used to fit the impedance spectrum, and the Chi sauared in the software is used to evaluate the fitting degree. The smaller the value is, the more it indicates that the fitted circuit is the same as the real circuit. And the Chi sauared value is more than 0.05, indicating that there is no correlation between the real circuit and the analog circuit. The X2 in the manuscript is far less than 0.05, indicating that the fitting circuit is the real circuit in the corrosion system. From Table 3, χ^2 is far less than 0.05.

From Fig. 8, the inhibition performance of molecules: SMIF > SMID. The increase in surface smoothness in the presence of SMIF and SMID molecules was further supported by the Bode plot. It can be seen from Fig. 8 that phase angle (α °) increases with an increase of inhibitors' concentration and the maximum increase in phase angle was −51.5° at the optimum concentration. However, for the ideal capacitor, the phase angle values −90° and the constant slope is −1. In the present study, the values of slope range from −0.4805 to

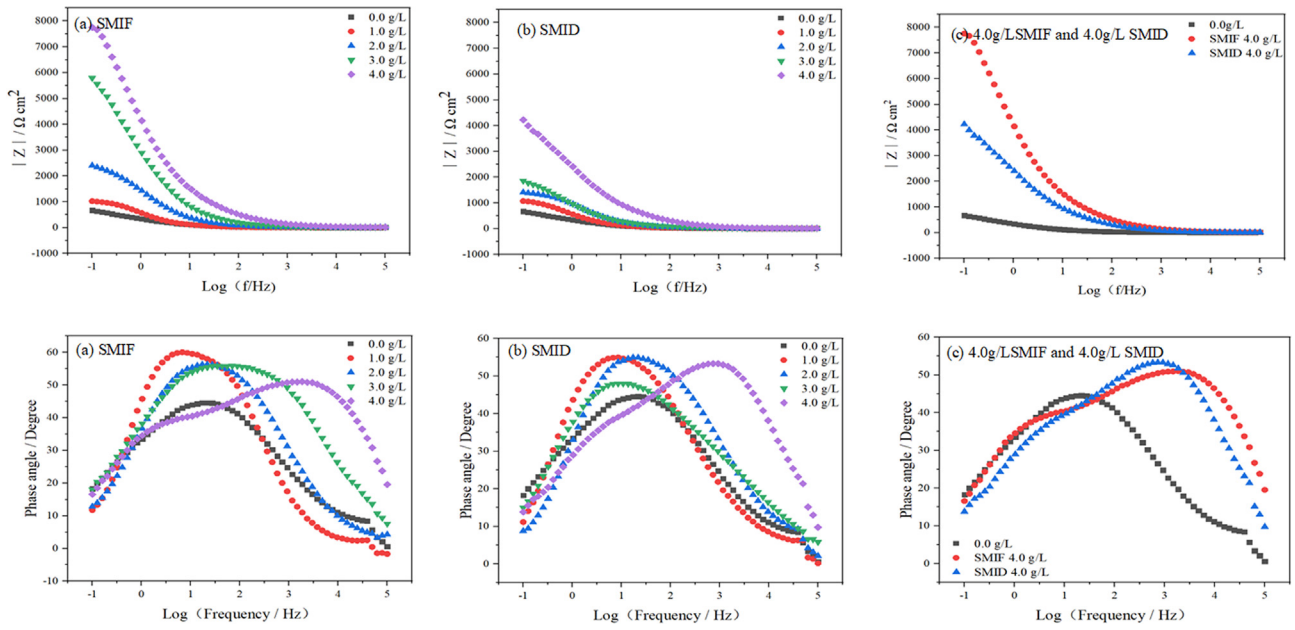

Fig. 8 Bode plots for carbon steel corrosion in SCP solution with different concentrations of SMIF and SMID.

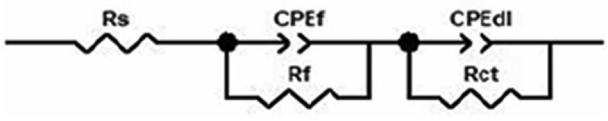

Fig. 9 Equivalent circuit for the analysis of the EIS data.

−0.7710, and the phase angle ranges from −41.30 to −51.5° (Tüken et al., 2012). It indicates that in the present analysis, the carbon steel interface did not behave as an ideal capacitor. The deviation from the ideal capacitive behavior is attributed to surface roughness (Goyal et al., 2018).

In Fig. 8(a), the corrosion resistance of carbon steel can be reflected by the low-frequency impedance modulus Z. the larger the impedance modulus Z, the better the corrosion resistance (Yadav et al., 2015). From Fig. 8(b), the phase angle φ increases with the increase of inhibitor concentration. The phase angle φ has a maximum value in high-frequency range, which indicates that inhibitor molecules can adsorb on the surface of carbon steel to form a protective film, it can effectively prevent corrosion.

It can be seen from Fig. 8(b), there are two peaks in phase angle φ, indicating that there are two reaction time constants; Fig. 7, Nyquist shows a capacitive circuit, and the impedance spectrum is basically consistent, indicating that the reaction mechanism of the electrode in SCP has not changed. The molecules of SMIF and SMID can adsorb on the surface of carbon steel in solution to form a protective film to further prevent corrosion of carbon steel surface by corrosive medium (Qiang et al., 2019).

3.6. Corrosion inhibitor adsorbed on steel surface

3.6.1. SEM analysis

Fig. 10 shows the morphology of carbon steel surfaces under different conditions. Fig. 10(a) shows carbon steel surface morphology dip in blank SCP solution for 5 days at 298 K. Fig. 10 (b) shows carbon steel surface morphology dip in 4 g/L SMID SCP for 5 days at 298 K. Fig. 10(c) shows carbon steel surface morphology dip in 4 g/L SMID SCP for 5 days at 298 K.

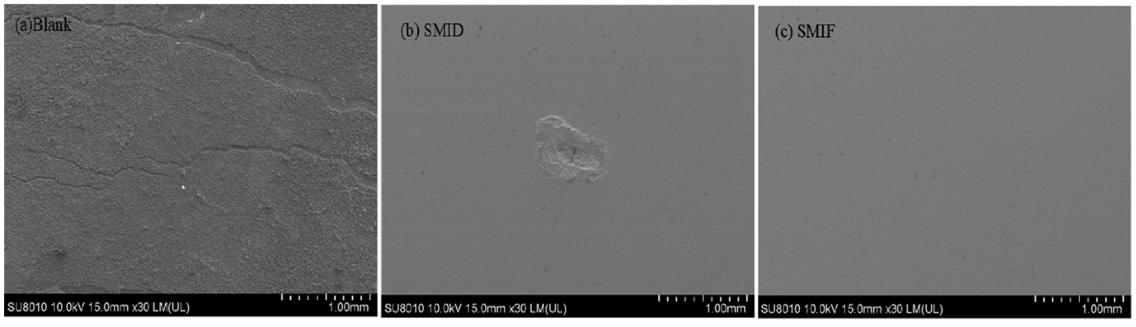

Fig. 10 (a) The surface of Q235 steel in SCP solution; (b) the surface of Q235 steel in 4.0 g/L SMIF; (c) the surface of Q235 steel in 4.0 g/L SMID.

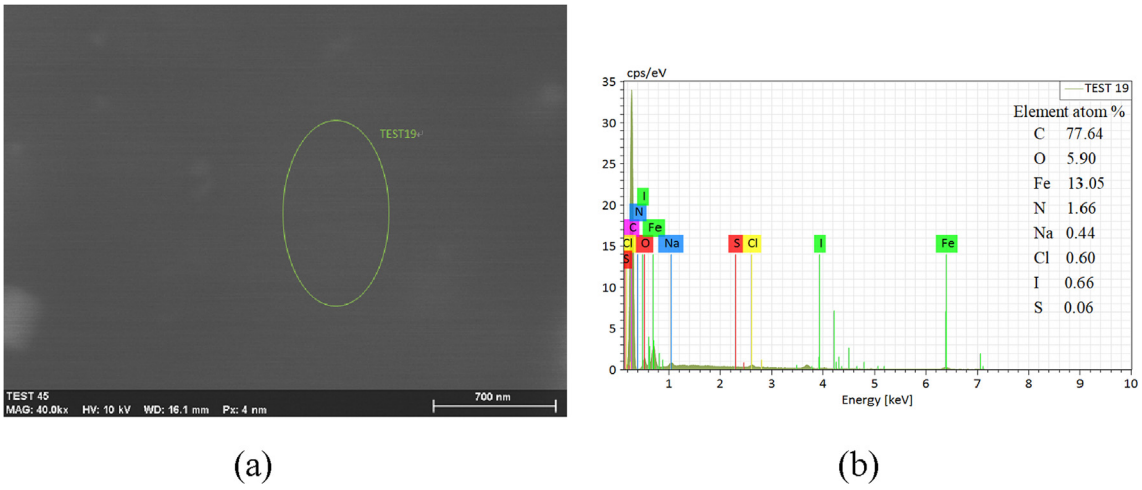

Fig. 11 (a) Surface of Q235 steel after corrosion (b) EDS energy spectra of green ellipse in Fig. 11a.

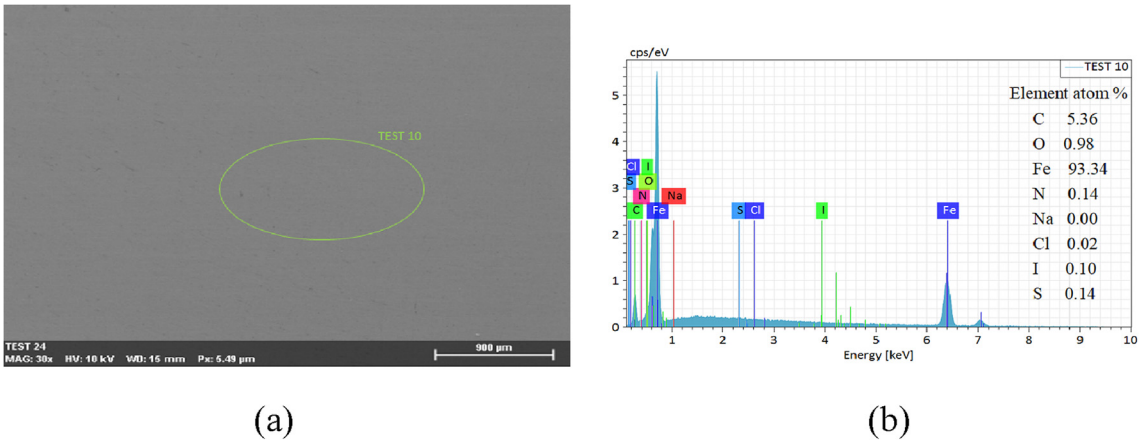

Fig. 12 (a) Surface of Q235 corrosion steel after cleaned (b) EDS energy spectra of green ellipse in Fig. 11a.

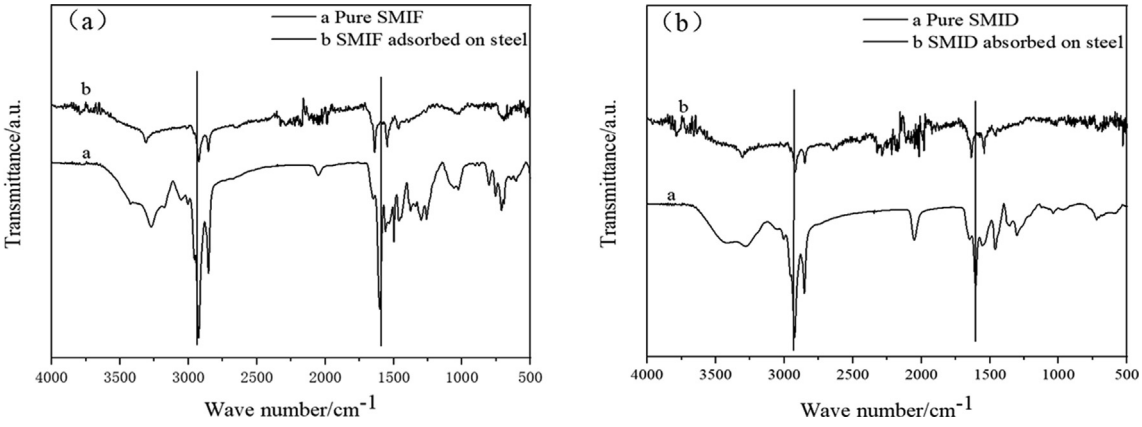

Fig. 13 The ATR-FTIR of pure corrosion inhibitor and corrosion inhibitor adsorbed on steel.

The surface of carbon steel shows obvious corrosion holes and seriously damaged in a blank SCP solution. In Fig. 10(b and c), it can be found that the corrosion degree on the surface of the Q235 is significantly reduced. The order of the flatness of carbon steel surface: SMIF > SMID > Blank.

In the SCP solution with SMIF and SMID inhibitor, a layer of film can be seen on clearly the surface of carbon steel. The morphology of the film and its EDS diagram and element analysis are shown in Fig. 11. The SEM diagram of film of the carbon steel surface after wiping and

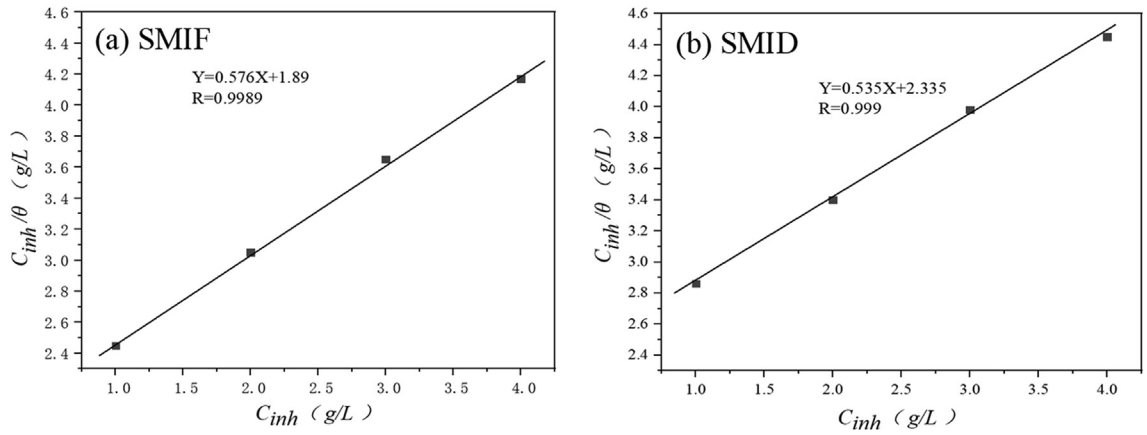

Fig. 14 Isothermal Langmuir fitting line for SMIF and SMID in SCP solution.

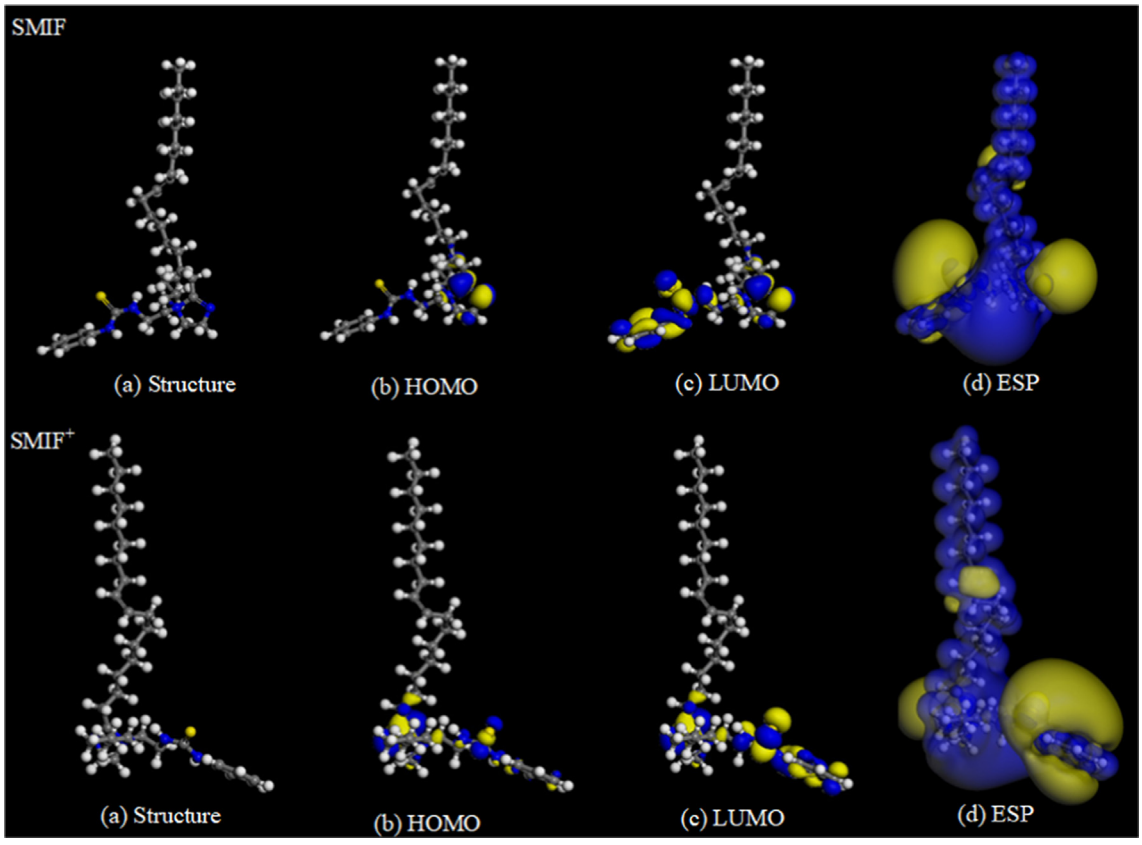

Fig. 15 Optimized configuration of SMIF, $SMIF^+$ and their frontier molecular orbital.

its EDS spectrum and the element analysis are displayed in Fig. 12.

From Figs. 11 and 12, in the SCP solution with corrosion inhibitor, the film uniformly covers the surface of carbon steel. After the film is wiped, the surface of carbon steel is even and smooth without obvious corrosion phenomenon. EDS shows that corrosion inhibitors element in the adsorption film on the surface of carbon steel. The carbon steel surface after wiping also contains inhibitor elements, which indicates that the adsorption film formed by inhibitor molecules, the film can prevent the corrosion medium adsorbing on the surface of Q235 and prevent the occurrence of corrosion effectively (Chugh et al., 2020).

3.6.2. ATR-Ftir

Infrared absorption spectroscopy is helpful in the general characterization of corrosion inhibitors structure. The corrosion inhibitor structures are revealed by the FTIR spectra of pure

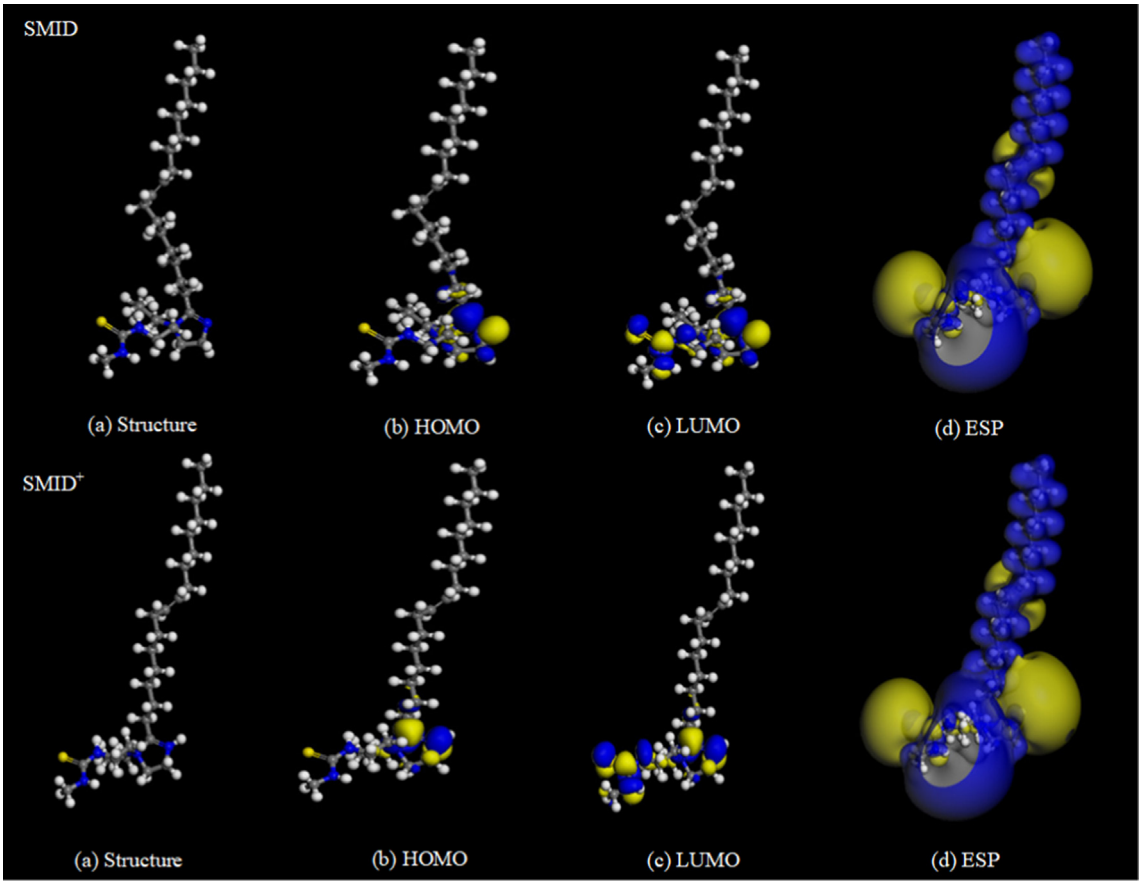

Fig. 16 Optimized configuration of SMID, $SMID^+$ and their frontier molecular orbital.

corrosion inhibitor and steel immersed in corrosive solution with corrosion inhibitor for 5 days as shown in Fig. 13 (Shubina et al., 2016).

The infrared spectra of the inhibitor molecules adsorbed on the steel surface and the pure inhibitor molecules have corresponding peaks at 3000 cm^{-1} and 1500 cm^{-1}, the formation of a corrosion inhibitive layer by SMIF and SMID adsorption on the mild steel surface is further confirmed (Javadian et al., 2017).

3.7. Adsorption isotherm model studies

Adsorption isotherms are of importance in evaluating the thermodynamic parameters of adsorption and understanding the possible mechanism of interaction between corrosion inhibitors and carbon steel surfaces. To clarify the nature of adsorption, several different adsorption isotherms (Langmuir, Temkin, Frumkin, etc.) were applied to evaluate the adsorption performance of inhibitors. Among these isotherms, the

Table 5 Quantum chemical values of corrosion inhibitor.

Inhibitor	E_{HOMO}	E_{LUMO}	ΔE
SMIF	−1.817	−1.188	0.629
SMID	−1.607	−0.773	0.834
$SMIF^+$	−2.186	2.130	0.056
$SMID^+$	1.620	0.602	1.018

Table 6 The adsorption energy of SMIF and SMID on Fe.

$E_{adsorption}$(kcal/mol)	Fe(1 1 0)	Fe(1 1 1)	Fe(0 0 1)
SMIF	−227.155	−43.660	−33.019
SMID	−103.637	−64.574	−21.527

Langmuir adsorption isotherm was ultimately found to best match the adsorption characteristics of the inhibitors, and the following Eq. (6):

$$C_{inh}/\theta = 1/K_{ads} + C_{inh} \quad (6)$$

where C_{inh} represents the inhibitor concentration, θ devotes the fraction of steel surface covered by inhibitor, which can be defined as $\theta = \eta_{weightloss}\%/100$ estimated, and K_{ads} represents the equilibrium constant of the whole adsorption process, which measure the strength of the adsorption forces between the inhibitor molecule and the carbon surface.

Generally, from the thermodynamics view, a larger inhibitor K value means a more efficient adsorption process and better inhibition performance. K value of SMIF and SMID is relatively high, implying that SMIF and SMID adsorbed on the carbon steel surface leads to high protection efficiency (El Aoufir et al., 2020).

The plot of C_{inh}/θ versus C_{inh} is shown in Fig. 14, the slope of which is useful for obtaining the K_{ads} value. The linear correlation coefficient (R^2) values of the inhibitors all reach above 0.99. In addition, the standard free energy (ΔG^0_{ads}) of inhibitor

adsorption on a metal surface, is calculated by the following Eq. (7):

$$\Delta G^{0}_{ads} = -RT\ln 55.5K_{ads} \quad (7)$$

where 55.5 denotes the value of the molar concentration of pure water, R, which equals to 8.314J(mol · K). represents the universal gas constant, and T is the temperature in Kelvin. ΔG^{0}_{ads} obtained from the Langmuir adsorption isotherm by weight loss for the adsorption of SMIF is −12.76 kJ· mol^{-1} and SMID is −11.44 kJ·mol^{-1}. Negative values of ΔG^{0}_{ads} indicate that the adsorption of the inhibitor onto the steel surface is accepted from the thermodynamics point of view and indicates the spontaneity of the adsorption process (Chafiq et al., 2020). In general, a more negative value of ΔG^{0}_{ads} implies the stronger trend of the adsorption strength of inhibitors adsorbing onto the metal surface. Furthermore, it is widely accepted that if $\Delta G^{0}_{ads}$is less negative than −20 kJ·mol^{-1}, it is identified as physical adsorption, or can be called electrostatic interaction happening between both the charged inhibitor molecules and the steel surface. However, if $\Delta G^{0}_{ads}$is more negative than −40 kJ·mol^{-1} it implies chemisorption, in this process, the inhibitor molecules are adsorbed onto the steel surface (Ferkous et al., 2020). In summary; Corrosion inhibitor molecules are physically adsorbed on the surface of carbon steel.

3.8. Theoretical studies

3.8.1. Quantum chemical calculation

The above experimental results show that SMIF and SMID adsorbs onto the steel surface via physical adsorption. It is necessary to acquire more information on the inherent nature of SMIF and SMID to understand the adsorption mechanisms on the carbon steel surface (Majd et al., 2019).

Figs. 15–16 shows that the electron donating region of SMIF and SMID inhibitor molecule is mainly located at C═S, and the active region for obtaining electrons is mainly distributed on the imidazole ring. SMIF molecule containing a phenyl can provide the certain electrons, which makes the SMIF molecules more incline to adsorb on the surface of Fe superior to SMID molecules. Quantum chemical calculated results are in well agreement with experimental results.

As regards the higher HOMO energy of an inhibitor molecule, it can be easier to donate electrons to the empty or unoccupied orbitals of the metal. Correspondingly, if the LUMO energy is lower, the inhibitor molecule can be easier to receive electrons from the metal. Therefore, lower values of ΔE are prone to get better inhibition efficiency. Energy band gap (E_{HOMO}-E_{LUMO} = ΔE) is perhaps the most important reactivity parameter and its low value is synonymous with high chemical reactivity and therefore high inhibition performance.

In the present analysis, values of ΔE obey the order: SMIF (0.629) < SMID(0.834). $SMIF^{+}$(0.056) < $SMID^{+}$(1.018), whether in the solvation or protonation, all consist with the order of inhibition efficiency determined by experiments. The Δ e value of SMIF in ionic liquid is the lowest, which indicates that SMIF is the softest and the most active, so it has the highest inhibition efficiency.

3.8.2. The molecular dynamics (MD) simulation

MD simulation was carried out for providing insightful information for adsorption mode of the corrosion inhibitor cations

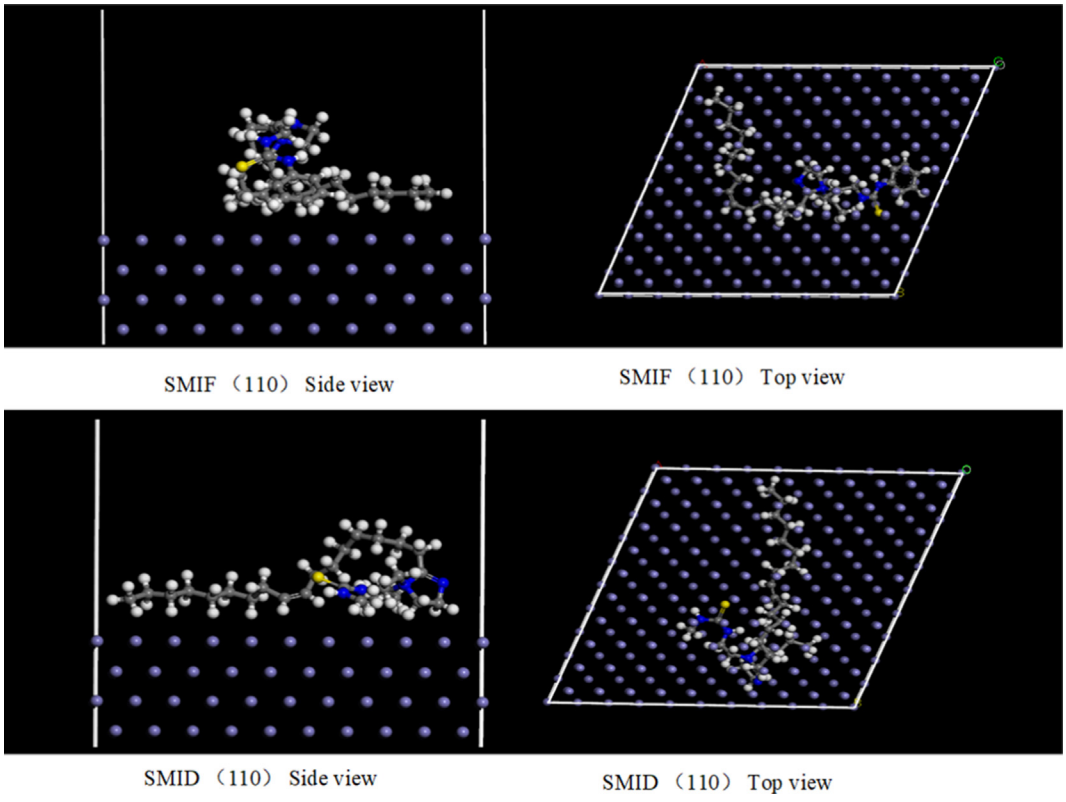

Fig. 17 The most stable configuration for the SMIF and SMID cation adsorption on the Fe (110), (111), (001) surface.

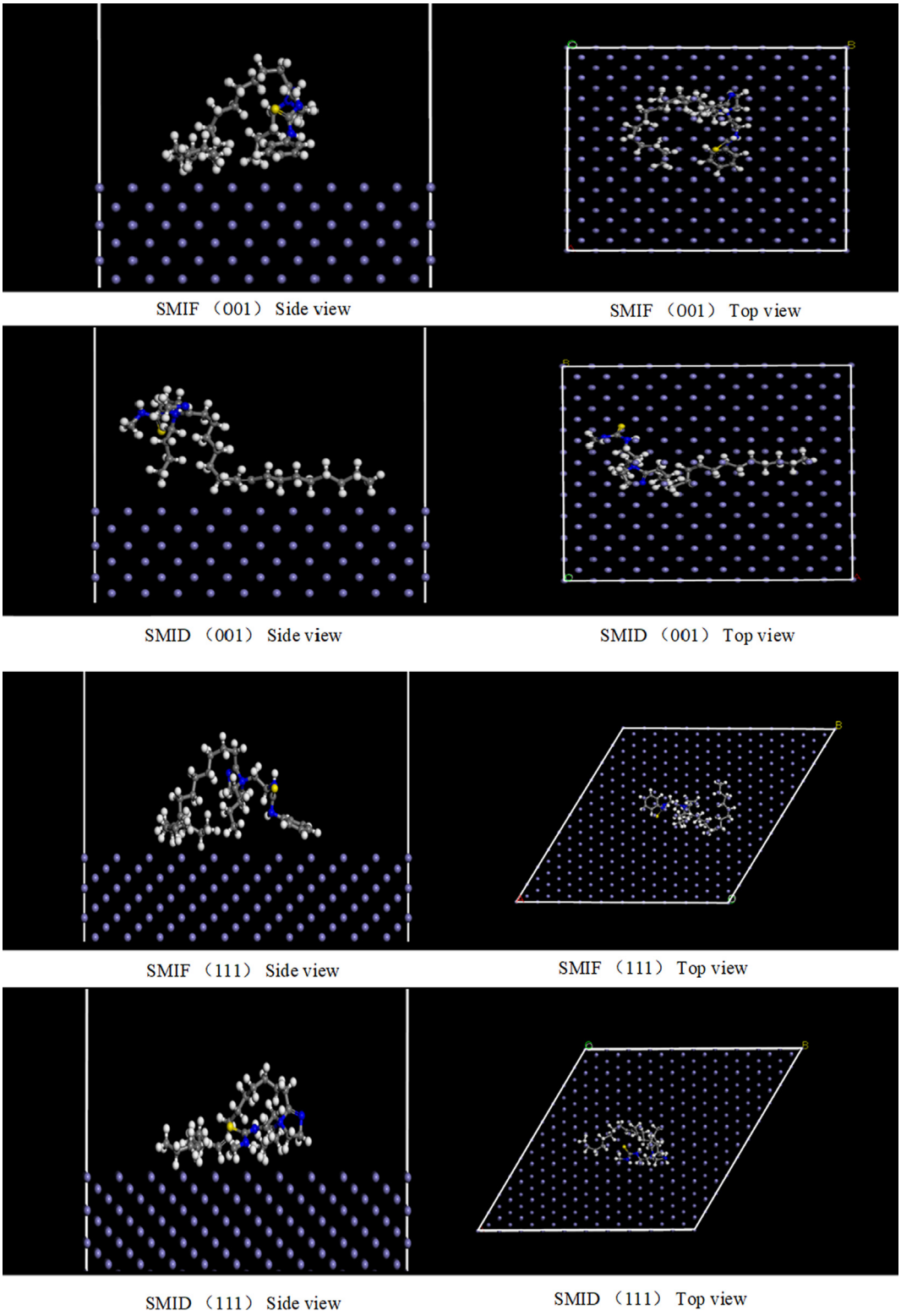

Fig. 17 (*continued*)

on the Fe surface and evaluating the interaction energy of the corrosion inhibitor with the Fe (110), (111), (001) surface (Chafiq et al., 2020; Verma et al., 2018).

MD simulation was carried out to provide an insightful information for adsorption mode of the cation of SMIF and SMID on the carbon steel surface and to evaluate the interac-

tion energy of inhibitor molecule with the Fe surface. The adsorption energy of SMIF inhibitor molecule and Fe can be calculated by Eq. (8), the more negative the value, the more stable the system and the better the corrosion inhibition performance of the molecule.

$$E_{adsorption} = E_{total} - (E_{surface} + E_{inhibitor}) \quad (8)$$

According to the molecular dynamics simulation, the adsorption energy is listed in Table 6.

Fig. 17 shows the equilibrium configuration for the adsorption state of the cation of SMIF and SMID on the Fe surface. It can be clearly seen that the favorite adsorbed sites of SMIF and SMID locate at imidazole ring and C=S bond, which can adsorb on the Fe surface effectively. Generally, the more negative adsorption energy means a stronger interaction between the adsorbent and adsorbate (Elgendy et al., 2019). The adsorption energies in Table 5 show that the adsorption strength of SMIF is superior to SMID. The calculated is results well supported by the experimental investigations.

4. Conclusions

In this work, we successfully fabricated two novel inhibitors, and their molecular structures were confirmed by IR, Raman spectroscopy and elemental analysis. The corrosion inhibition performance was proved by weight loss experiment and electrochemical experiment. The inhibition mechanism was studied by DFT and molecular dynamics simulation. The main conclusions can be drawn as follows:

(1) The results of weight loss test show that SMIF exhibits better inhibition effect than that of SMID, and the inhibition efficiency of SMIF could reach 96.02%. The inhibition efficiency of these two inhibitors increases with increasing the concentration of inhibitors.
(2) Electrochemical test results exhibit that the open circuit potential show that the inhibitor is an anode type inhibitor and can form an adsorption film on the steel surface. Potentiodynamic polarization show that the corrosion inhibitor molecules formed protective film on the surface of carbon steel, which also prevented the charge transfer. The electrochemical impedance spectroscopy further proves that the inhibitor molecule belongs to anode type inhibitor molecule.
(3) EDS and FTIR showed that the inhibitor molecules existed on the surface of carbon steel, and the adsorption isotherm proved that the inhibitor belonged to Langmuir adsorption, which is consistent with the conclusion of electrochemistry. The conclusion is also confirmed by computational chemistry.

This investigation would give a positive guidance for our future work.

Declaration of Competing Interest

The authors declare that they have no known competing financial interests or personal relationships that could have appeared to influence the work reported in this paper.

Acknowledgments

The authors acknowledge the financial support provided by the National Natural Science Foundation of China (51965020, 51605336 and 21563012); Jiangxi Science Foundation of China (20202BAB204020, 20202BABL204045, 20171BCD40009, 20181BAB203010); Jiangxi Provincial Education Department Foundation of China (GJJ190319, GJJ180305).

References

Aquino-Torres, E., Camacho-Mendoza, R.L., Gutierrez, E., et al, 2020. The influence of iodide in corrosion inhibition by organic compounds on carbon steel: theoretical and experimental studies. Appl. Surf. Sci. 514.
Asadi, N., Ramezanzadeh, M., Bahlakeh, G., et al, 2020. Theoretical MD/DFT computer explorations and surface-electrochemical investigations of the zinc/iron metal cations interactions with highly active molecules from Lemon balm extract toward the steel corrosion retardation in saline solution. J. Mol. Liq. 310.
Bashir, S., Thakur, A., Lgaz, H., et al, 2020. Corrosion inhibition efficiency of bronopol on aluminium in 0.5 M HCl solution: Insights from experimental and quantum chemical studies. Surf. Interfaces 20.
Berisha, A., 2020. Experimental, monte carlo and molecular dynamic study on corrosion inhibition of mild steel by pyridine derivatives in aqueous perchloric acid. Electrochem 1 (2), 188–199.
Cao, S., Liu, D., Zhang, P., et al, 2017. Green Bronsted acid ionic liquids as novel corrosion inhibitors for carbon steel in acidic medium. Sci. Rep. 7 (1), 8773.
Cao, S., Liu, D., Ding, H., et al, 2019. Corrosion inhibition effects of a novel ionic liquid with and without potassium iodide for carbon steel in 0.5 M HCl solution: an experimental study and theoretical calculation. J. Mol. Liq. 275, 729–740.
Chafiq, M., Chaouiki, A., Damej, M., et al, 2020. Bolaamphiphile-class surfactants as corrosion inhibitor model compounds against acid corrosion of mild steel. J. Mol. Liq. 309.
Chen, C., Jiang, L., Guo, M.-Z., et al, 2019. Effect of sulfate ions on corrosion of reinforced steel treated by DNA corrosion inhibitor in simulated concrete pore solution. Constr. Build. Mater. 228.
Chugh, B., Singh, A.K., Chaouiki, A., et al, 2020. A comprehensive study about anti-corrosion behaviour of pyrazine carbohydrazide: gravimetric, electrochemical, surface and theoretical study. J. Mol. Liq. 299.
Douche, D., Elmsellem, H., Anouar, E.H., et al, 2020. Anti-corrosion performance of 8-hydroxyquinoline derivatives for mild steel in acidic medium: gravimetric, electrochemical, DFT and molecular dynamics simulation investigations. J. Mol. Liq. 308.
El Aoufir, Y., Aslam, R., Lazrak, F., et al, 2020. The effect of the alkyl chain length on corrosion inhibition performances of 1,2,4-triazole-based compounds for mild steel in 1.0 M HCl: insights from experimental and theoretical studies. J. Mol. Liq. 303.
El Faydy, M., Galai, M., El Assyry, A., et al, 2016. Experimental investigation on the corrosion inhibition of carbon steel by 5-(chloromethyl)-8-quinolinol hydrochloride in hydrochloric acid solution. J. Mol. Liq. 219, 396–404.
Elgendy, A., Elkholy, A.E., El Basiony, N.M., et al, 2019. Monte Carlo simulation for the antiscaling performance of Gemini ionic liquids. J. Mol. Liq. 285, 408–415.
El-Hajjaji, F., Messali, M., Aljuhani, A., et al, 2018. Pyridazinium-based ionic liquids as novel and green corrosion inhibitors of carbon steel in acid medium: electrochemical and molecular dynamics simulation studies. J. Mol. Liq. 249, 997–1008.

El-Shamy, A.M., Zakaria, K., Abbas, M.A., et al, 2015. Anti-bacterial and anti-corrosion effects of the ionic liquid 1-butyl-1-methylpyrrolidinium trifluoromethylsulfonate. J. Mol. Liq. 211, 363–369.

Ferkous, H., Djellali, S., Sahraoui, R., et al, 2020. Corrosion inhibition of mild steel by 2-(2-methoxybenzylidene) hydrazine-1-carbothioamide in hydrochloric acid solution: Experimental measurements and quantum chemical calculations. J. Mol. Liq. 307.

Finšgar, M., 2020. Electrochemical, 3D topography, XPS, and ToF-SIMS analyses of 4-methyl-2-phenylimidazole as a corrosion inhibitor for brass. Corros. Sci. 169.

Goyal, M., Vashisht, H., Kumar, S., et al, 2018. Anti-corrosion performance of eco-friendly inhibitor (2-aminobenzyl) triphenylphosphonium bromide ionic liquid on mild steel in 0.5 M sulfuric acid. J. Mol. Liq. 261, 162–173.

Guerrab, W., Lgaz, H., Kansiz, S., et al, 2020. Synthesis of a novel phenytoin derivative: crystal structure, Hirshfeld surface analysis and DFT calculations. J. Mol. Struct. 1205.

Guo, L., Zhu, S., Li, W., et al, 2015. Electrochemical and quantum chemical assessment of 2-aminothiazole as inhibitor for carton steel in sulfuric acid solution. Asian J. Chem. 27 (8), 2917–2923.

Javadian, S., Darbasizadeh, B., Yousefi, A., et al, 2017. Dye-surfactant aggregates as corrosion inhibitor for mild steel in NaCl medium: experimental and theoretical studies. J. Taiwan Inst. Chem. Eng. 71, 344–354.

Kousar, K., Ljungdahl, T., Wetzel, A., et al, 2019. An exemplar imidazoline surfactant for corrosion inhibitor studies: synthesis, characterization, and physicochemical properties. J. Surfactants Deterg. 23 (1), 225–234.

Liu, Q., Song, Z., Han, H., et al, 2020. A novel green reinforcement corrosion inhibitor extracted from waste Platanus acerifolia leaves. Constr. Build. Mater. 260.

Majd, M.T., Bahlakeh, G., Dehghani, A., et al, 2019. Combined molecular simulation, DFT computation and electrochemical studies of the mild steel corrosion protection against NaCl solution using aqueous Eucalyptus leaves extract molecules linked with zinc ions. J. Mol. Liq. 294.

Padash, R., Sajadi, G.S., Jafari, A.H., et al, 2020. Corrosion control of aluminum in the solutions of NaCl, HCl and NaOH using 2,6-dimethylpyridine inhibitor: experimental and DFT insights. Mater. Chem. Phys. 244.

Pakiet, M., Tedim, J., Kowalczyk, I., et al, 2019. Functionalised novel gemini surfactants as corrosion inhibitors for mild steel in 50 mM NaCl: experimental and theoretical insights. Colloids Surf. A: Physicochem. Eng. Asp., 580

Pan, C., Chen, N., He, J., et al, 2020. Effects of corrosion inhibitor and functional components on the electrochemical and mechanical properties of concrete subject to chloride environment. Constr. Build. Mater. 260.

Qiang, Y., Zhang, S., Zhao, H., et al, 2019. Enhanced anticorrosion performance of copper by novel N-doped carbon dots. Corros. Sci. 161.

Qiang, Y., Zhang, S., Wang, L., 2019. Understanding the adsorption and anticorrosive mechanism of DNA inhibitor for copper in sulfuric acid. Appl. Surf. Sci. 492, 228–238.

Qiang, Y., Li, H., Lan, X., 2020. Self-assembling anchored film basing on two tetrazole derivatives for application to protect copper in sulfuric acid environment. J. Mater. Sci. Technol. 52, 63–71.

Qiang, Y., Guo, L., Li, H., et al, 2021. Fabrication of environmentally friendly Losartan potassium film for corrosion inhibition of mild steel in HCl medium. Chem. Eng. J. 406.

Rbaa, M., Ouakki, M., Galai, M., et al, 2020. Simple preparation and characterization of novel 8-Hydroxyquinoline derivatives as effective acid corrosion inhibitor for mild steel: experimental and theoretical studies. Colloids Surf. A: Physicochem. Eng. Asp., 602

Sahoo, S., Nayak, S., Sahoo, D., et al, 2019. Corrosion inhibition behavior of dual phase steel in 3.5 wt % NaCl solution by carica papaya peel extracts. Mater. Today:. Proc. 18, 2642–2648.

Saraswat, V., Yadav, M., Obot, I.B., 2020. Investigations on eco-friendly corrosion inhibitors for mild steel in acid environment: electrochemical, DFT and Monte Carlo Simulation approach. Colloids Surf. A: Physicochem. Eng. Asp., 599

Shubina, V., Gaillet, L., Chaussadent, T., et al, 2016. Biomolecules as a sustainable protection against corrosion of reinforced carbon steel in concrete. J. Cleaner Prod. 112, 666–671.

Singh, A., Ansari, K.R., Kumar, A., et al, 2017. Electrochemical, surface and quantum chemical studies of novel imidazole derivatives as corrosion inhibitors for J55 steel in sweet corrosive environment. J. Alloys Compd. 712, 121–133.

Singh, A., Ansari, K.R., Quraishi, M.A., et al, 2020. Theoretically and experimentally exploring the corrosion inhibition of N80 steel by pyrazol derivatives in simulated acidizing environment. J. Mol. Struct. 1206.

Tan, J., Guo, L., Yang, H., et al, 2020. Synergistic effect of potassium iodide and sodium dodecyl sulfonate on the corrosion inhibition of carbon steel in HCl medium: a combined experimental and theoretical investigation. RSC Adv. 10 (26), 15163–15170.

Tan, B., Zhang, S., Liu, H., et al, 2019. Corrosion inhibition of X65 steel in sulfuric acid by two food flavorants 2-isobutylthiazole and 1-(1,3-Thiazol-2-yl) ethanone as the green environmental corrosion inhibitors: combination of experimental and theoretical researches. J. Colloid Interface Sci. 538, 519–529.

Tan, B., Zhang, S., Qiang, Y., et al, 2020. Experimental and theoretical studies on the inhibition properties of three diphenyl disulfide derivatives on copper corrosion in acid medium. J. Mol. Liq. 298.

Tan, B., Xiang, B., Zhang, S., et al, 2021. Papaya leaves extract as a novel eco-friendly corrosion inhibitor for Cu in H2SO4 medium. J. Colloid Interface Sci. 582 (Pt B), 918–931.

Tüken, T., Demir, F., Kıcır, N., et al, 2012. Inhibition effect of 1-ethyl-3-methylimidazolium dicyanamide against steel corrosion. Corros. Sci. 59, 110–118.

Verma, C., Obot, I.B., Bahadur, I., et al, 2018. Choline based ionic liquids as sustainable corrosion inhibitors on mild steel surface in acidic medium: gravimetric, electrochemical, surface morphology, DFT and Monte Carlo simulation studies. Appl. Surf. Sci. 457, 134–149.

Wang, P., Wang, Y., Zhao, T., et al, 2020. Effectiveness protection performance of an internal blending organic corrosion inhibitor for carbon steel in chloride contaminated simulated concrete pore solution. J. Adv. Concr. Technol. 18, 116–128.

Xu, W., Wei, J., Yang, Z., et al, 2020. Feasibility and corrosion inhibition efficacy of zeolite-supported lauric acid imidazoline as corrosion inhibitor in cementitious mortar. Constr. Build. Mater. 250.

Yadav, M., Kumar, S., Sinha, R.R., et al, 2015. New pyrimidine derivatives as efficient organic inhibitors on mild steel corrosion in acidic medium: electrochemical, SEM, EDX, AFM and DFT studies. J. Mol. Liq. 211, 135–145.

Yan, T., Zhang, S., Feng, L., et al, 2020. Investigation of imidazole derivatives as corrosion inhibitors of copper in sulfuric acid: combination of experimental and theoretical researches. J. Taiwan Inst. Chem. Eng. 106, 118–129.

Ye, Y., Zhang, D., Zou, Y., et al, 2020. A feasible method to improve the protection ability of metal by functionalized carbon dots as environment-friendly corrosion inhibitor. J. Cleaner Prod. 264.

Yu, Z., Liu, Y., Liang, L., et al, 2019. Inhibition performance of a multi-sites adsorption type corrosion inhibitor on P110 steel in acidic medium. Chem. Phys. Lett. 735.

Zhang, Z., Ba, H., Wu, Z., 2019. Sustainable corrosion inhibitor for steel in simulated concrete pore solution by maize gluten meal extract: Electrochemical and adsorption behavior studies. Constr. Build. Mater. 227, 117080.